Martensitic transition during Ni growth on Fe(001): evidence of a precursor phase



2012 New J. Phys. 14 053048

(http://iopscience.iop.org/1367-2630/14/5/053048)

New Journal of Physics
The open-access journal for physics

# Martensitic transition during Ni growth on Fe(001): evidence of a precursor phase

**G Bussetti[1], M Riva, A Picone, A Brambilla, L Duò, M Finazzi and F Ciccacci**

CNISM, NEMAS and Dipartimento di Fisica, Politecnico di Milano, Piazza Leonardo da Vinci 32, I-20133 Milano, Italy
E-mail: gianlorenzo.bussetti@polimi.it

*New Journal of Physics* **14** (2012) 053048 (12pp)
Received 29 February 2012
Published 31 May 2012
Online at http://www.njp.org/
doi:10.1088/1367-2630/14/5/053048

**Abstract.** We report evidence that the body-centered cubic (bcc)–face-centered cubic (fcc) transition that occurs during Ni film growth on a Fe(001) substrate is preceded by a pre-martensitic phase, as demonstrated by low-energy electron diffraction. The corresponding film superstructure is characterized by a displacement of Ni atoms along the main ⟨100⟩ crystallographic axes of iron, without any rotation of the unit cell with respect to the (001) plane, in contrast with the martensitic transition that shows four fcc Ni domains with the Ni⟨211⟩ crystallographic directions aligned with the Fe⟨110⟩ axes. In addition, the martensitic transition is detected not at 6 ML, as previously believed, but above 20 ML if the Ni sample is rigorously kept at room temperature. The surface morphology of the bcc–fcc transition is characterized by the development of Ni mounds oriented along the ⟨110⟩ directions, as shown by scanning tunneling microscopy.

[1] Author to whom any correspondence should be addressed.

## Contents



## 1. Introduction

The electronic and magnetic properties of solids are strongly influenced by their crystallographic structure [1]. Small changes in lattice parameters or distortions of the unit cells have a direct effect on the main physical characteristics of a sample [2]. Consequently, it might be possible to continuously tune the electronic (e.g. the metal–semiconductor transition [3]) and magnetic properties of a system [2] just by stretching the interatomic distances and modifying the orbital overlaps. This possibility has been a strong motivation for numerous studies in solid state physics, aiming to stabilize metastable phases of matter in the attempt to create new materials with selected properties. Some elements, such as iron, naturally show diverse allotropic phases with opposite magnetic characteristics at different critical temperatures. For instance, the Fe body-centered cubic (bcc) crystal structure ($\alpha$-Fe) is the most stable phase of iron in standard conditions and is ferromagnetic. In contrast, the iron face-centered cubic (fcc) crystal structure (austenite or $\gamma$-Fe) is paramagnetic but is observed only at temperatures above 1180 K. Conversely, nickel shows an fcc structure and no other allotropes are observed at higher temperatures.

One of the most successful and well-established approaches for obtaining metastable crystals, even in standard conditions, is to grow thin films over a template, typically a clean and well-defined surface of a crystalline substrate. In fact, the complex equilibrium between the energy costs of crystal cell distortion and the energy gain in the film–substrate interface formation may allow the growing film to stabilize in a metastable crystallographic structure, at least up to a critical thickness above which the film typically relaxes by undergoing plastic deformations.

In this context, thin films, multilayers and interfaces involving the late 3*d* transition metals (e.g. Fe and Ni) have stimulated interest in many studies, due to the need for designing artificial materials with improved magnetic, magneto-optic and magneto-transport properties that can play a key role in many technological applications. Such materials have also proved to be important in understanding the fundamental properties of mutually interacting thin films as well as the microscopic details of the film structure during the relaxation from the pseudomorphic phase to the stable structure [4].

The system consisting of a thin Ni film on Fe is very promising for applications, since Fe carries a higher magnetic moment than Ni, while the latter, thanks to its higher electronegativity, is better suited than Fe to withstand oxidation. A thorough characterization of the structural

properties of thin Ni films on Fe thus represents a crucial step to understanding the physics of such systems.

The crystallographic structure of pseudomorphic Ni thin films grown on the Fe(001) surface is characterized by the bcc phase [5], which is expected to be non-magnetic. Although the evolution of Ni films on Fe(001) has been studied as a function of thickness for more than two decades both experimentally [6, 7] and theoretically [8], there are still details of the growth mechanisms that need to be further investigated [9]. In particular, the bcc–fcc transition (martensitic transition) in Ni/Fe(001) films seems to occur abruptly above a critical thickness of 6 ML [5], while many other bcc–fcc and fcc–bcc transitions (see [4] and references therein) show a precursor phase.

The current state-of-the-art of the Ni/Fe interface formation can be summarized as follows. (i) Up to 6 ML (1 ML being the number of Ni atoms necessary to fill every Fe(001) hollow site (i.e. $1.217 \times 10^{15}$ atoms cm$^{-2}$), whose nominal thickness has been determined by using the expected density of bcc Ni), the Ni film has a pseudomorphic bcc structure with an in-plane lattice parameter of 2.87 Å (Fe bulk) instead of 2.77 Å, as predicted by theoretical calculations for bcc Ni [10, 11]. The expansion causes a contraction of the interplanar spacing in the Ni overlayer. Such a contracted spacing has been observed to be 1.35 Å [12, 13]. (ii) Above 6 ML the Ni film undergoes a sudden phase transition from the bcc to the fcc structure. This transition is characterized by a specific $c(2 \times 2)$-like reconstruction in the diffraction patterns (e.g. [14] high-energy electron diffraction (RHEED)), which is interpreted in terms of four different domains, each exposing the (110) plane of the fcc structure and oriented as described by the Nishiyama–Wassermann path of the martensitic transition [15]. (iii) Density functional theory (DFT) calculations [8] suggest that the Ni film undergoes a cell rotation with respect to the Fe(001) bare substrate, at about 3–4 ML. This finding is compatible with a $c(2 \times 2)$-like reconstruction, as mentioned above [14]. In addition, simulations based on DFT and molecular dynamics stress that the Ni/Fe interface is highly unstable above 300/400 K and that film growth needs to be carried out at low temperatures (room temperature (RT) or lower) to avoid Ni inter-diffusion inside the substrate.

In this work, we show that, in samples kept at RT, the bcc–fcc transition occurs at a sample thickness much larger than any reported so far, taking place above 20 ML. This seems to reconcile the experimental findings with the homogeneous strain theory, which predicts a critical thickness for the bcc Ni overlayer of about 25 ML [16]. Moreover, a new precursor phase is unambiguously identified in 10–20-ML-thick Ni/Fe(001) films by low-energy electron diffraction (LEED). The precursor phase is characterized by a distortion of the Ni superstructure along the main Fe crystallographic axes, namely [100] and [010], and no unit cell rotation is detected. A scanning tunneling microscopy (STM) investigation of the film shows that the martensitic transition is accompanied by the formation of Ni mounds oriented along the ⟨110⟩ directions, in agreement with the other bcc–fcc transitions reported in the literature [17–21].

## 2. Experimental details

Measurements have been carried out in an ultra-high vacuum (UHV—base pressure in the $10^{-9}$ Pa range) apparatus with Ar-ion sputtering, LEED, Auger electron spectroscopy (AES) and STM (Omicron®) facilities. Clean Fe(001) substrates are prepared by depositing a thick Fe film on an MgO(001) single crystal according to a standard protocol [22]. The Fe(001) substrate shows a sharp $(1 \times 1)$ square LEED pattern and small roughness with large terraces separated

by 1-ML-high steps as seen by STM [23, 24]. Ni is evaporated at near normal incidence by an e-beam cell located at about 15 cm from the substrate. A chromel–alumel (type K) thermocouple is positioned in close proximity to the sample in order to monitor its temperature during each preparation step. The Ni-cell flux has been carefully calibrated by using a quartz microbalance and checked by AES and STM. A stable flux of 0.8 ML $min^{-1}$ has been chosen for our experiments, in agreement with previous studies [5]. During Ni growth the pressure in the preparation chamber did not exceed $3 \times 10^{-8}$ Pa. Ni films with different thicknesses have been grown at RT following two alternative strategies: (i) by depositing a given amount of Ni each time on a freshly prepared Fe surface, as obtained by sputter-removal of the previous Ni film followed by annealing; (ii) by adding a new amount of Ni to the previous deposition step after full characterization by AES, LEED and STM. No significant changes have, however, been detected by following either strategy (i) or (ii). No contaminants were observed in the Auger spectra, which consisted of Ni and Fe peaks, the latter showing a reduction with the overlayer thickness, well consistent with uniform growth with no interdiffusion [25].

## 3. Results

Figure 1 summarizes our experimental results obtained on the Ni/Fe(001) system as the Ni thickness is progressively increased from 0 (clean Fe(001)) to 6, 20 and 40 ML (rows (a)–(b), (c)–(d), (e)–(f) and (g)–(h), respectively), whose nominal thicknesses have been determined by using the expected density of bcc Ni, in agreement with the literature.

In the first column, we show the LEED images collected on our samples. A well-defined $(1 \times 1)$ symmetry pattern is observed in figure 1(a) on the freshly prepared Fe(001) substrate. Figure 1(b) illustrates an STM image of a substrate region ($160 \times 160\,nm^2$), showing the presence of monoatomic steps. At a nominal coverage of 6 ML, the coalescence of the islands of the topmost layer creates large flat areas (see figure 1(d)). LEED indicates strictly pseudomorphic growth, as the diffraction pattern is still of $(1 \times 1)$ symmetry (see section 4.1), and spot positions coincide with those of Fe(001) (figure 1(c)). The quality of the LEED pattern is not significantly degraded despite the increased roughness of the epitaxial growth, although the LEED background intensity was slightly enhanced. A similar experimental result has been described in the pseudomorphic growth of $\gamma$-Fe on Ir(001) [4]. In figure 1(d), three different layers are clearly visible from our STM data, suggesting a multilayer growth mode of the Ni film at this coverage regime.

The same $(1 \times 1)$ diffraction pattern is detected in each Ni deposition step from 6 ML up to 10 ML (not reported here), the only difference being an increase of the scattered background and a smearing of the diffraction spots.

For Ni thickness above 10 ML the LEED background significantly increases and spots (10), (01), $(\bar{1}0)$ and $(0\bar{1})$ show an enhancement of diffused light along the main crystallographic axes of iron. Deeper analysis of LEED images proves that some extra spots appear as satellites of the substrate main spots. These satellites gradually gain intensity as the Ni film thickness is increased up to 20 ML, suggesting that the structural change highlighted by LEED affects several buried layers and not only the topmost one. The final visible effect is the appearance of cross-like features (see figure 1(e)). Conversely, spots (11), $(\bar{1}1)$, $(\bar{1}\bar{1})$ and $(1\bar{1})$ are not visible and no satellites are detected. This is probably due to the increasing sensitivity to local disorder and surface roughness of the LEED spots with increasing Miller indices. Incidentally, we note that just at this coverage a coexistence of satellites and fading $c(2 \times 2)$-like extra spots

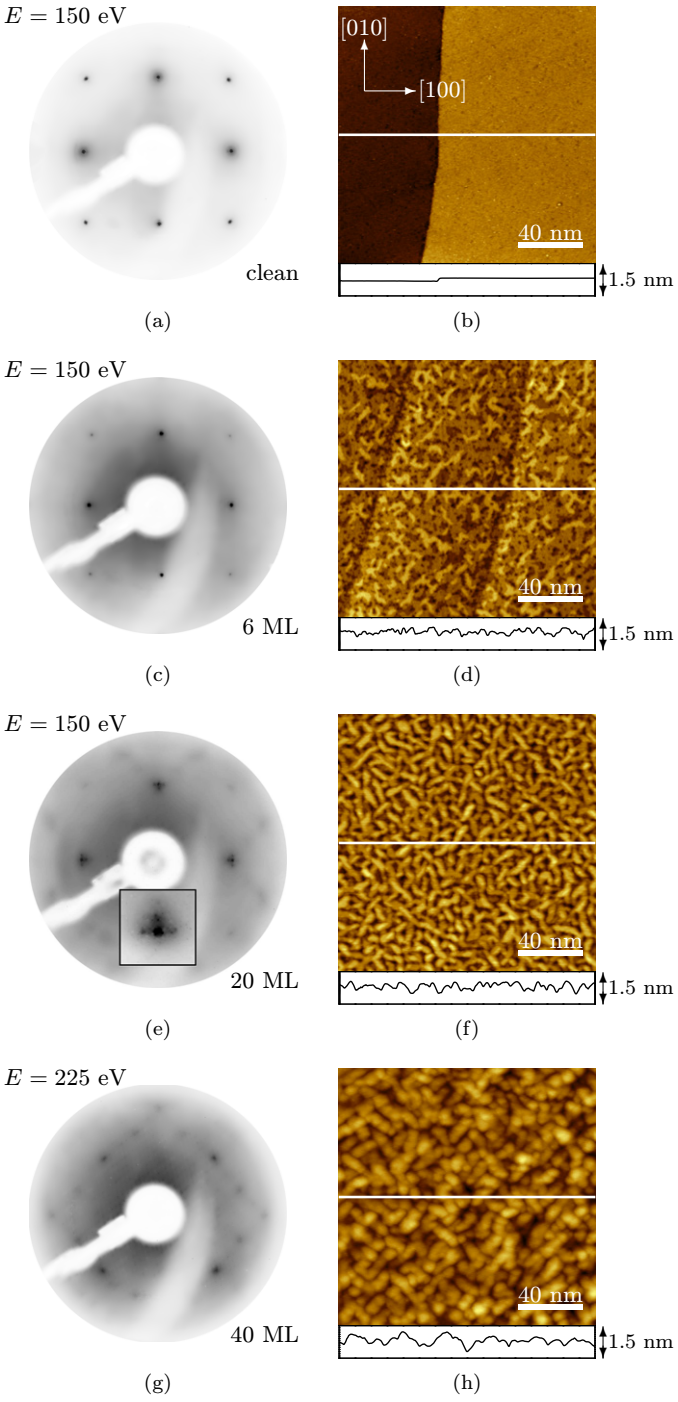


**Figure 1.** Rows are related to the clean Fe(001), 6, 20 and 40 ML of Ni film from top to bottom, respectively. In the left column, the corresponding LEED patterns (electron beam energy $E = 150$ eV in panels (a), (c) and (e), $E = 225$ eV in panel (g)) are reported. In panel (e); a blow-up of the satellites around the $(0\bar{1})$ diffraction spot (see text) is reported. LEED pictures have been acquired by a digital camera with an integration time of 30 s. The right column collects the STM images and related profiles, acquired along the horizontal line ($I_{\text{tunnel}} = 1$ nA; $V_{\text{bias}} = 1$ V).

is detected. Figure 1(f) reports a typical STM image of a 20-ML-thick Ni film grown at RT. A system of mounds decorates the overall surface. Each mound is a few layers high, as can be inferred from the line profile.

Above 20 ML, the satellites disappear from the LEED pattern and a clear $c(2 \times 2)$-like reconstruction is observed, replacing the original $(1 \times 1)$ (see figure 1(g)). The $c(2 \times 2)$-like symmetry has been reported in the literature [14] and is attributed to the development of a fcc phase for the Ni film following the martensitic transition. However, the critical thickness obtained in this work differs from those obtained by several other authors [5, 12–14], according to whom the martensitic transition occurs at 6 ML, although in close agreement with the homogeneous strain theory [16], which predicts a critical thickness for the bcc Ni overlayer around 25 ML. We believe that the reason for such a discrepancy has to be looked for in the sample temperature. In our measurements, we carefully kept the temperature constant at 300 K, while other strategies have been used and reported in the literature [5, 14] (in other works the sample temperature might have risen above RT). Consequently, our data indicate that the bcc–fcc transition at RT takes place at a higher film thickness than previously believed, namely 20 ML instead of 6 ML, which was the commonly accepted value. A rapid inspection of figure 1(h) reveals that some changes are evident also in the surface morphology. The mounds, already observed at 20 ML, are now larger in size and seem to be preferentially oriented along the ⟨110⟩ diagonals of the main [100] and [010] iron axes. Despite this increase in size, it was not possible to achieve atomic resolution on these mounds, which is, however, quite a common situation in STM on metals at RT. Nevertheless, Ni mounds generate a nice fabric-like texture with domains that closely resemble characteristic martensitic micro- and nanostructures observed by optical microscopy [26] and STM [27], respectively.

We have followed the Ni growth up to a thickness of 100 ML. No other significant changes with respect to the situation at 40 ML were detected. At higher thicknesses, LEED spots had a lower intensity and broader shape than at lower coverages, while the film morphology always showed a stable texture with a roughness (about 180 pm) comparable with that characterizing the 40 ML Ni film.

## 4. Discussion

### *4.1. Film structure*

In many bcc–fcc and fcc–bcc transitions observed in thin films growing on a template, the film crystal structure undergoes changes that are driven by the energetic gain obtained by relieving the surface stress, which originates from an imperfect match between the lattice parameter of the substrate and that of the growing film. In particular, the growth of both Ni and Fe on crystal surfaces usually proceeds through complex structural changes, associated with the appearance of different surface reconstructions or with a particular evolution of their magnetic characteristics [17–21]. Even the growth of Fe on Ni(001) displays interesting phenomenological features in both its structure and morphology [28].

Regarding Ni film growth on Fe(001) at RT,[2] the presence of satellites around the main $(1 \times 1)$ LEED spots in the Ni coverage range between 10 and 20 ML also proves that such a system is characterized by an intermediate structural change (never observed until now), before the martensitic transition is completed. In the following, we present an analysis of the satellite

[2] The precursor phase, described in this work, is visible even at 120 °C.

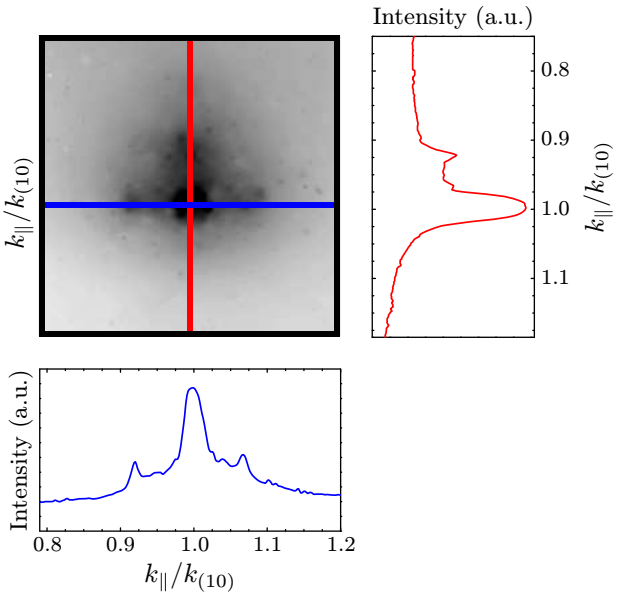


**Figure 2.** Intensity profiles of a magnified view of the inset of figure 1(e), represented as a function of the relative scattering vector ($k_{\|}/k_{(10)}$). Two satellites are visible from the horizontal LEED intensity profile (blue line), while a single satellite is detected in the vertical profile (red line).

structure and a simulation of the LEED pattern in order to understand the microscopic change that occurs in the Ni film before the bcc–fcc transition.

It has been demonstrated that, when a sample is mechanically stressed, the $(1 \times 1)$ pattern is modified [29] so that each diffracted spot is surrounded by a symmetric halo. It is reasonable to think that even our sample, when it is close to the critical thickness for the bcc–fcc transition (namely 20 ML), can experience high values of local surface stress that would explain the observed LEED. However, as already mentioned, a closer inspection of the inset of figure 1(e) shows that the halo has a cross-like shape and is actually constituted by at least three extra spots aligned along the main [100] and [010] directions. Such an observation is confirmed by an additional analysis of the LEED intensity profiles along the $\langle 100 \rangle$ directions in the proximity of the $\{10\}$ spots, summarized in figure 2. This finding is in good agreement with similar systems that exhibit a fcc–bcc transition [17–21]. However, the martensitic family is wide and comprises different materials with specific peculiarities. Some of them show pretransitional phenomena known as 'tweed' (see [30] and references therein) characterized by symmetric solid lines in the diffraction pattern [31]. Consequently, our LEED pattern excludes the 'tweed' phase and implies that the intermediate phase is a real precursor (also pre-martensitic) phase during which Ni atoms are stressed along the main [100] and [010] directions of the pseudomorphic bcc phase. Such a pre-martensitic phase is usually interpreted in terms of the so-called sine-like deformation model [17–21] that predicts the displacements of the surface atoms from a pseudomorphic position to assume the form of a sinusoidal wave, with the displacements along a crystallographic axis whose periodicity is equal to an integer multiple of the in-plane lattice constant of the underlying substrate.

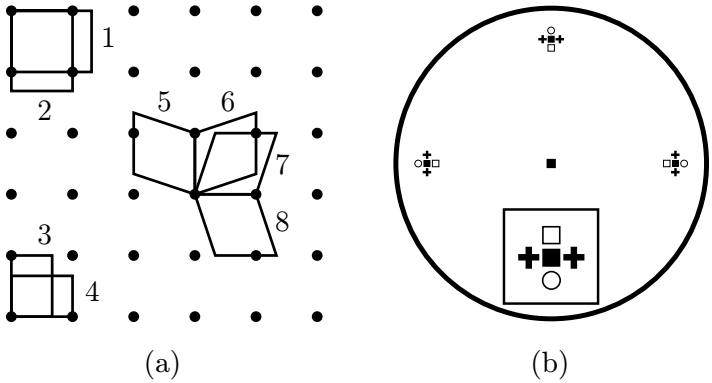


**Figure 3.** (a) Different Ni cells that are considered to interpret the experimental LEED pattern. (1) A stretched unit cell; (2) point symmetry group (only a 90° rotation) applied to the cell (1); (3) a contracted unit cell; (4) point symmetry group (only a 90° rotation) applied to the cell (3); (5) cell obtained by a displacement of Ni atoms along a crystallographic direction of Fe, due to the effect of a shear stress; (6)–(8) cells obtained from (5) by applying systematically all the operators of the 4*mm* point symmetry group of the square. (b) LEED simulation result (Sim4tec). Symbols (filled squares, open squares, open circles and black crosses) refer to the position of spots and satellites in the LEED screen. The inset shows a blow-up of the satellites around the $(\bar{1}0)$ diffraction spot. Filled squares refer to the $(1 \times 1)$ symmetry pattern. Open squares are linked to Ni cells (1) and (2); open circles refer to cells (3) and (4), not observed experimentally, while black crosses originate from Ni cells (5)–(8).

In order to prove our statement, we have simulated (Sim4tec) the observed LEED pattern by using two Ni supercell distortions that can be considered a simpler version of the sine-like deformation model.

If we consider a distorted superstructure (with respect to the lattice of the (001) surface), we can notice that the possible shifts of the Ni atoms must follow any path which is compatible with the 4*mm* point symmetry group of the square, the only restriction being that each single atom shifts along the crystallographic axes (see figure 1(e)). Consequently, the main distortions of a square lattice domain are just two: (i) stretching (or contraction), which changes a square domain into a rectangular one and it is due to an axial stress; (ii) dislocation, which is due to a shear stress and changes a square lattice into an oblique one. Figure 3 summarizes all possible Ni cell distortions. The result is a collection of eight surface cells, where the distance of the displaced Ni atoms is 0.2 Å with respect to the unperturbed position. In principle, there is no reason to prefer one domain with respect to another one. Consequently, we can initially consider our eight domains as equiprobable.

It is realistic to think that the overall surface tessellation is a collection of domains obtained by coupling the above eight cells, consistent with the sine-like model and a consequent low cost in terms of surface energy.

Figure 3(b) shows that the simulated diffraction pattern is in very good agreement with the experimental data reported in figure 1(e). However, from the above-reported simulation, satellites related to the contracted cells ((3) and (4) in figure 3(a)) are not visible experimentally

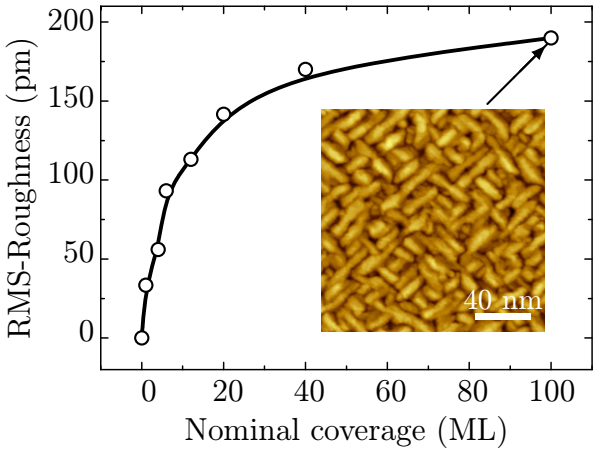


**Figure 4.** Surface roughness (rms), calculated on $160 \times 160\,\mathrm{nm}^2$ STM images, as a function of the nominal Ni film thickness. The open circles represent experimental data, while the full line is a guide to the eyes. Inset: an STM image ($160 \times 160\,\mathrm{nm}^2$) acquired on the sample with a nominal Ni coverage of 100 ML ($I_{\mathrm{tunnel}} = 1\,\mathrm{nA}$; $V_{\mathrm{bias}} = 1\,\mathrm{V}$).

(cf figure 1(e)), suggesting that tensile and shear stresses predominate in the Ni superstructure deformation. This means that, by comparing experimental data and simulations, we can infer that the main mechanisms that govern the precursor phase are tensile and shear stresses and that compression plays a minor role.

We can thus conclude that the Ni super-cell structure undergoes a pre-martensitic transformation, characterized by a shift of Ni atoms along the main crystallographic axes of iron. This phase closes, on the one hand, the pseudomorphic growth of Ni on Fe(001) and, on the other, it is qualitatively different from the true martensitic transition because the latter is characterized by a rotation of the supercells with respect to the bare substrate, which we did not observe in our LEED patterns below a nominal Ni thickness of 20 ML. This finding reconciles the difference of the bcc–fcc transition of Ni on Fe with respect to other systems such as, for example, Fe films grown on Ni [28], which are characterized by a complex evolution of both structure and morphology.

### *4.2. Film morphology*

Figure 4 reports the dependence of the overall surface roughness as a function of thickness.

Such an evolution is in agreement with the multilayer growth of a film, as already reported in the literature [28]. Below 10 ML, the roughness seems to increase almost linearly and then there is a change in the trend. Probably, this is due to the stress relaxation that shifts the Ni atoms along the [100] direction (described above as a specific characteristic of the pre-martensitic phase, occurring for coverages above 10 ML) and the overall effect of stress relief is to reduce the rate of surface roughness increase with film thickness. Above 20 ML, the evolution reported in figure 4 tends to saturate. It is worth noting that when a stable structure is obtained above 20 ML (Ni fcc phase), also the film morphology reflects a stationary situation. This is particularly true if one compares the STM image for a 40-ML-thick Ni film (figure 1(g)) with that related to a coverage of 100 ML (see the inset of figure 4). Both images are characterized by a nice fabric-like texture and no significant differences are observed.

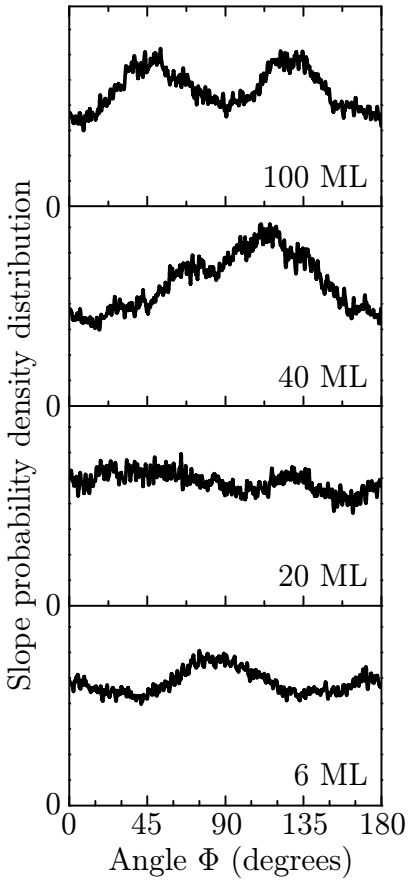


**Figure 5.** Slope probability density distribution of Ni domains and mounds at four different film coverages (from the bottom to the top: 6, 20, 40 and 100 ML). In the picture, 0°, 45° and 90° correspond to a mound orientation along the [100], [110] and [010] directions, respectively. The slope distribution has been calculated on $160 \times 160\,\mathrm{nm}^2$ STM images. The zero probability density is reported for clarity in each panel.

We analyzed the probability density function (Gwyddion) associated with the preferential orientation of the Ni crystal mounds of four different film thicknesses (namely 6, 20, 40 and 100 ML) [32] and the results are summarized in figure 5, where 0°, 45° and 90° correspond to the alignment of Ni mounds along the [100], [110] and [010] directions, respectively. The angular distribution of the mounds in the 6 ML sample shows a periodic trend with maxima at 0°, 90° and 180°. This result indicates that, during the pseudomorphic film growth, the Ni domains evolution follows the main crystallographic axes of iron. Incidentally, we note that only the Ni topmost layer displays islands with borders aligned along the bcc ⟨110⟩ directions, which is a morphological peculiarity of the Ni fcc phase (see below). The distribution is significantly changed during the precursor phase (namely up to 20 ML). No relevant structures can be detected in the angular distribution for the 20-ML-thick film, which shows almost flat behavior. The precursor phase, as mentioned in section 4.1, is characterized by Ni cell distortions that can produce changes in the orientation of the mounds with respect to the iron axes that correspond to a flattening of the calculated distribution, as observed in figure 5, 20 ML.

After the martensitic transition, the angular distribution of the mounds shows new features, centered around $90^\circ \pm 10^\circ$. The broad shape of such a feature could be a consequence of the increased surface roughness, as reported in figure 4. At 100 ML, when a nice fabric-like texture is definitely observed (see the inset of figure 4), two clear structures at 45° and 135° are obtained in the angular distribution, corresponding to a mound orientation along the ⟨110⟩ directions. In this respect, we recall that Mijiritskii *et al* [14] recognized that their four equivalent Ni cells, which are in agreement with the Nishiyama–Wassermann transition path, can produce domains with boundaries aligned exactly along the bcc ⟨110⟩ directions. Our STM results support this interpretation from a morphological point of view and help in the comprehension of the fourfold symmetry observed by Heinrich *et al* [33, 34] in the magnetic properties of the Ni/Fe(001) system.

## 5. Conclusions

In conclusion, in this work we have reported clear evidence for a pre-martensitic phase during the growth of Ni on Fe(001), as recognized by LEED analysis. It is important to underline that the growth was performed strictly at RT. The pre-martensitic phase, which closes the true Ni pseudomorphic regime, is characterized by a lattice deformation along the [100] and [010] directions, due to tensile and shear stresses, that produces cross-shaped satellites around the main LEED spots. The diffraction pattern has been interpreted in the framework of the sine-like deformation model, in agreement with other precursor phases reported in the literature. The martensitic bcc–fcc transition, which occurs with increasing sample thickness, is delayed with respect to what is reported so far, taking place at thicknesses above 20 ML. In addition, inspection of the film morphology shows that the Nishiyama–Wassermann transition path produces a nice fabric-like texture, with Ni mounds aligned along the ⟨110⟩ directions, that covers the entire surface. Our findings can be useful for the current debate about the microscopic changes that occur in the formation of the Ni/Fe interface [8].

Moreover, one of the results of this work is the possibility of growing a thin bcc Ni layer that can be used as a stable buffer layer in temperature (up to 400 K) and in thickness (up to 20 ML). For instance, it is known that, due to the strong lattice misfit (about 19%) between pure Ni and NiO, thin NiO films do not grow epitaxially on Ni substrates. This might be relevant for the field of surface magnetism, for instance to realize thin metal oxide films coupled to magnetic substrates [35], which can be problematic when the substrate is less electronegative than the overlayer and is thus easily oxidized. In this respect, a bcc Ni buffer layer can avoid the oxidation of e.g. a Fe substrate, opening up a real chance to extend the existing palette of sharp oxide–substrate interfaces.

## Acknowledgments

This work was partially supported by the Italian Ministry of University and Research through the FIRB project RBAP115AYN.

## References

[1] Prinz G 1985 *Phys. Rev. Lett.* **54** 1051–4

[2] Shen J, Lin M-T, Giergiel J, Schmidthals C, Zharnikov M, Schneider C M and Kirschner J 1996 *J. Magn. Magn. Mater.* **156** 104–6

[3] Nistor M, Gherendi F, Mandache N B, Hebert C, Perrière J and Seiler W 2009 *J. Appl. Phys.* **106** 103710–7
[4] Martin V, Meyer W, Giovanardi C, Hammer L, Heinz K, Tian Z, Sander D and Kirschner J 2007 *Phys. Rev.* B **76** 205418
[5] Wang Z Q, Li Y, Jona F and Marcus P 1987 *Solid State Commun.* **61** 623–6
[6] Vaz C A F, Bland J A C and Lauhoff G 2008 *Rep. Prog. Phys.* **71** 056501
[7] Myagkov V G, Zhigalov V C, Bykova L E and Bondarenko G N *J. Magn. Magn. Mater.* **305** 534
[8] Hashibon A, Schravendijk P, Elsässer C and Gumbsch P 2009 *Phil. Mag.* **89** 3413–33
[9] Finlayson T R and Klemradt U 2005 Martensitic transformations at surfaces and interfaces *Proc. Int. Conf. on Solid–Solid Phase Transformations in Inorganic Materials (Phoenix, AZ, USA, 29 May–3 June 2005)* vol 2 ed J M Howe, D E Laughlin, J K Lee, U Dahmen and W A Soffa (Warrendale, PA: Minerals, Metals and Materials Society) pp 35–46
[10] Moruzzi V L, Marcus P, Schwarz K and Mohn P 1986 *Phys. Rev.* B **34** 1784–91
[11] Mishin Y, Mehl M J and Papaconstantopoulos D A 2005 *Acta Mater.* **53** 4029–41
[12] Kamada Y and Matsui M 1997 *J. Phys. Soc. Japan* **66** 658–63
[13] Kamada Y, Matsui M and Asada T 1997 *J. Phys. Soc. Japan* **66** 466–71
[14] Mijiritskii A, Smulders P, Chumanov V, Rogojanu O, James M and Boerma D 1998 *Phys. Rev.* B **58** 8960–6
[15] Sandoval L, Urbassek H M and Entel P 2009 *New J. Phys.* **11** 103027
[16] Chernov A A 1984 *Modern Crystallography III: Crystal Growth* (Berlin: Springer)
[17] Müller S, Bayer P, Kinne A, Reischl C, Metzler R and Heinz K 1995 *Surf. Sci.* **331–333** 723–30
[18] Müller S, Bayer P, Reischl C, Heinz K, Feldmann B, Zillgen H and Wuttig M 1995 *Phys. Rev. Lett.* **74** 765–8
[19] Daum W, Stuhlmann C and Ibach H 1988 *Phys. Rev. Lett.* **60** 2741–4
[20] Heinz K, Müller S and Bayer P 1996 *Surf. Sci.* **352–354** 942–50
[21] Heinz K, Müller S and Hammer L 1999 *J. Phys.: Condens. Matter* **11** 9437–54
[22] Bertacco R and Ciccacci F 1999 *Phys. Rev.* B **59** 4207–10
[23] Picone A *et al* 2010 *Phys. Rev.* B **81** 115450–6
[24] Picone A, Brambilla A, Calloni A, Duò L, Finazzi M and Ciccacci F 2011 *Phys. Rev.* B **83** 235402–8
[25] Bussetti G, Riva M, Picone A, Brambilla A, Duò L, Ciccacci F and Finazzi M 2012 Thermal instability of thin Ni/Fe(001) films *Nanosci. Nanotechnol. Lett.* accepted
[26] Liu Z, Wu G and Liu Y 2006 *Intermetallics* **14** 1493–500
[27] Methfessel T and Elmers H J 2007 *Surf. Sci.* **601** 5026–33
[28] Shen J, Schmidthals C, Woltersdorf J and Kirschner J 1998 *Surf. Sci.* **407** 90–103
[29] Sander D, Tian Z and Kirschner J 2009 *J. Phys.: Condens. Matter* **21** 134015
[30] Lloveras P, Castán T, Porta M, Planes A and Saxena A 2009 *Phys. Rev.* B **80** 054107
[31] Saxena A, Castán T, Planes A, Porta M, Kishi Y, Lograsso T A, Viehland D, Wuttig M and De Graef M 2004 *Phys. Rev. Lett.* **92** 197203
[32] Riva M 2011 Ultrathin nickel films on iron: a scanning tunneling microscopy investigation *Master Thesis* Politecnico di Milano
[33] Heinrich B, Purcell S T, Dutcher J R, Urquhart K B, Cochran J F and Arrott A S 1988 *Phys. Rev.* B **38** 12879–96
[34] Heinrich B, Cochran J F, Arrott A S, Purcell S T, Urquhart K B, Dutcher J R and Egelhoff W F 1989 *Appl. Phys.* A **49** 473–90
[35] Finazzi M, Duò L and Ciccacci F 2009 *Surf. Sci. Rep.* **64** 139–67